Electronic Supplementary Material (ESI) for RSC Advances.
This journal is © The Royal Society of Chemistry 2014

Supporting Information

A One-step Practical Strategy to Enhance Overall Pseudocapacitor Performance

Sun-I Kim, Kyeong-Nam Kang, Sung-Wook Kim, and Ji-Hyun Jang*
Interdisciplinary School of Green Energy, 689-798, UNIST, Korea

Preparation of the Ni(OH)$_2$ based electrodes and NiSCC

The SCC was fabricated by electrodeposition of nickel on the as-prepared electrodes. In order to fabricate the control electrode, synthesized powders (Ni(OH)$_2$, 85 wt%) were mixed with acetylene black (5 wt%) and polyvinylidene difluoride (PVDF, 10 wt%). 1.2 mg of the mixture was then pasted onto an etched Ni plate and dried at 150°C in an air atmosphere for 12 hours. The precursor solution for Ni-deposition was prepared in a mixture of 66 g/L $NiSO_4$, 9 g/L $NiCl_2$, and 7 g/L H_3BO_3 in D.I water. The as-prepared electrode was dipped into the Ni-precursor solution and electrodeposited at a constant current (-10 mA) condition for various times from 1 min s to 5 min to form NiSCC. The carbon grid and the Ag/AgCl reference electrode were used as a counter electrode and reference electrode, respectively. After Ni-deposition, the Ni-deposited electrode was fully washed to remove remaining precursor solutions, and then the samples were dried at 120°C for 12 hours under vacuum.

Electrochemical Measurements

The electrochemical performance of the Ni(OH)$_2$ electrode with SCC was evaluated using Pt foil as a counter electrode and a KOH solution (1 M) as an electrolyte. The electrochemical properties were conducted by galvanostatic charge−discharge and cyclic voltammetry using a computer controlled electrochemical interface (VMP3 biologic) from 0.1 V to 0.65 V at room temperature. EIS data were obtained at a frequency range from 100 kHz to 0.1 Hz using a potentiostat (Versa STAT 3, AMETEK).

Characterization

The structures of synthesized $Ni(OH)_2$ and electrodes were characterized using FE-SEM (SEM, FEI/USA Nanonova 230) and high-resolution TEM (FETEM, JEOL TEM 2100) at an accelerating voltage of 200 kV. The crystallinity of the electrodes was checked using a X-ray diffraction system (Bruker D8 Advance system) with Cu Ka radiation ($\lambda = 1.5406$ A) at a scan rate of 2 °/min the 2θ range from 10° to 80°. The specific surface area, pore size, and pore volume were analyzed using the Brunauer-Emmett-Teller (BET) method with a Belsorp max system (Bel Japan).

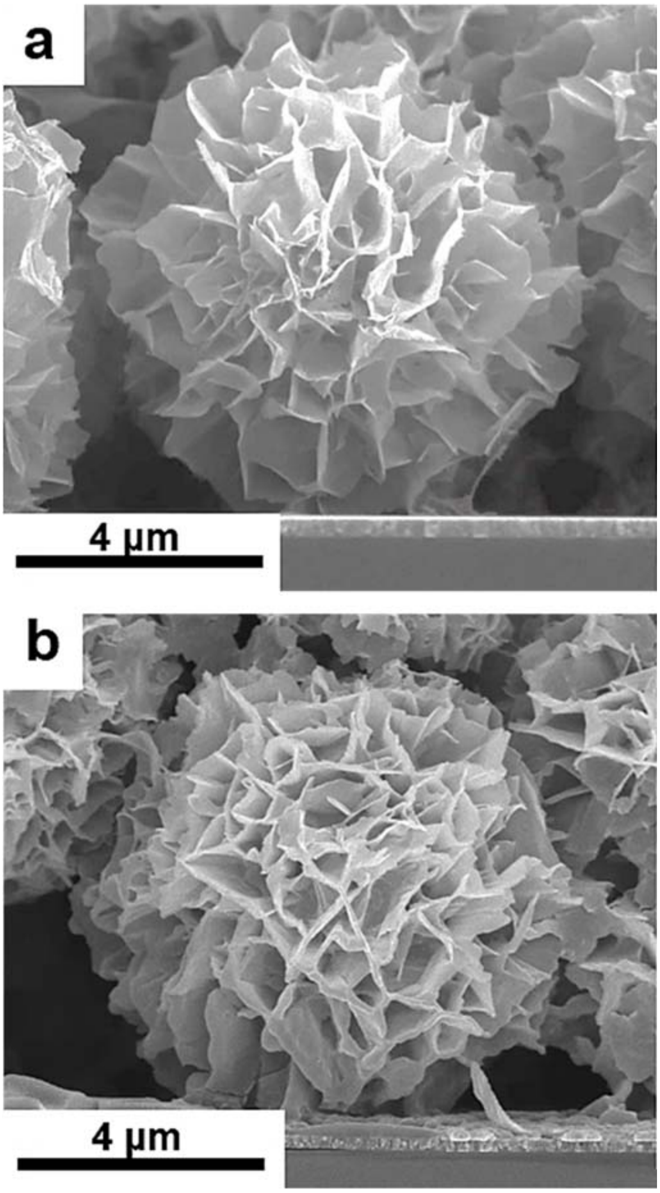

Figure S1. Morphological characterization of as-synthesized hierarchical nickel hydroxide structures before and after Ni-electrodepositon: cross-sectional SEM image of devices based on $Ni(OH)_2$ (a); cross-sectional SEM image of devices based on NiSCC-$Ni(OH)_2$ (b).

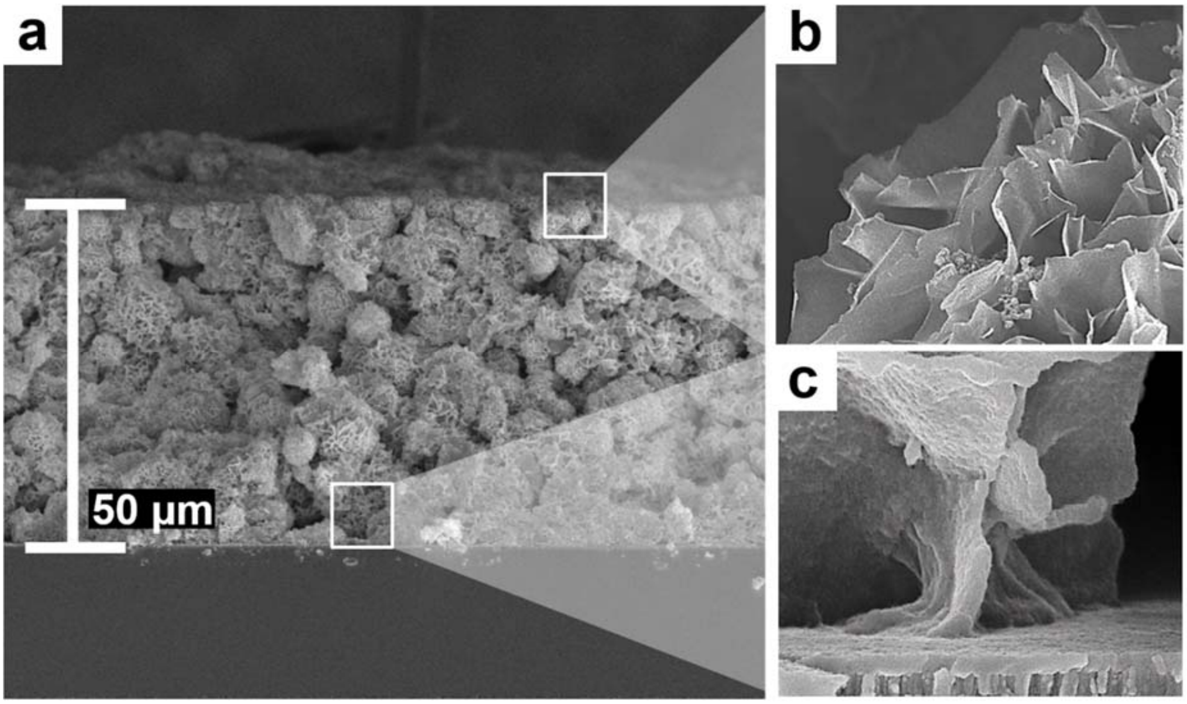

Figure S2. The cross-sectional SEM images of the electrode based on Ni(OH)$_2$ powder after Ni-electrodeposition for 2 min. (a); Top part of the electrode (b).; Bottom part of the electrode (c).

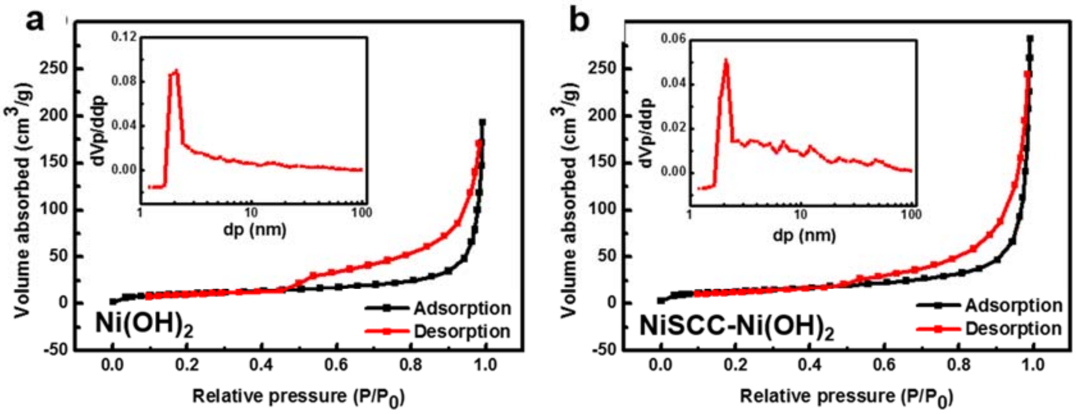

	Surface area (m^2/g)	Pore size (nm)	Pore volume (cm^3/g)
$Ni(OH)_2$	35.51	31.30	0.27
NiSCC-$Ni(OH)_2$	45.54	35.53	0.40

Figure S3. N_2 adsorption-desorption isotherm loop of the $Ni(OH)_2$ electrode before (a) and after Ni-electrodeposition for 2 min. (b) The inset shows the BJH pore size distribution curve of each electrode.

The surface properties of active materials play a key role in the performance of supercapacitors, because ions in electrolytes are mainly stored on the surface of the active materials. In general, as higher surface area is provided, more electroactive sites become active for efficient Faradaic redox reaction, leading to higher specific capacitance. Figure S3 shows the BET data of the $Ni(OH)_2$ electrode before and after Ni-deposition. In order to compare the exact active area of the fabricated devices, samples for BET measurement were prepared by gathering scratched materials after preparing the electrode first. The surface area of the as-prepared $Ni(OH)_2$ electrode was 35.51 m^2/g, whereas the surface area of the active electrodes after Ni-deposition increased up to ~30%, 45 m^2/g), accompanied by an increase of the pore volume and pore size. This is likely because Ni-NPs create a rougher surface and pores of $Ni(OH)_2$ slightly decomposed under the acidic condition for Ni.

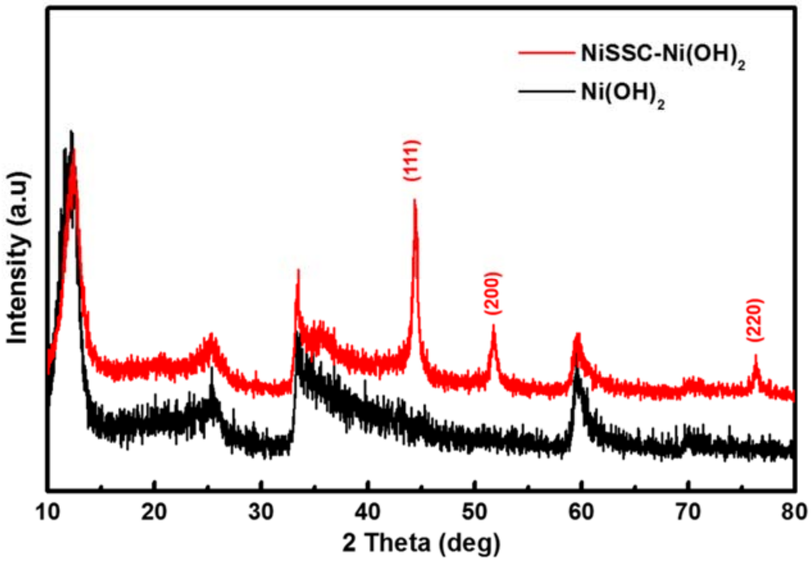

Figure S4. XRD patterns of $Ni(OH)_2$ electrode (in black) and $Ni(OH)_2$ electrode with NiSCC (in red).

The as-prepared $Ni(OH)_2$ powders were characterized on the basis of the XRD patterns, as shown in Figure S4. The black curve indicates the peaks of $Ni(OH)_2$ electrodes while the red line represents the XRD pattern of $Ni(OH)_2$ electrodes after Ni-deposition. The crystallinity of the as-synthesized $Ni(OH)_2$ powders was identified as α-phase (JCPDS, 038-0715) in the form of the turbostatic disordered structure with peak positions at $2\theta = 11.6^{o}$, 22.9^{o}, 34.2^{o} and 59.8^{o} corresponding to the plane of (003), (006), (012), and (110) of $Ni(OH)_2$, respectively. After Ni-electrodeposition, strong peaks at $2\theta = 44^{o}$, 52^{o}, and 76^{o}, which were indexed to the (111), (200), and (220) planes of Ni (JCPDS, 070-1849), appeared while the original peaks of $Ni(OH)_2$ were retained, which proved that no impurities were incorporated into $Ni(OH)_2$.

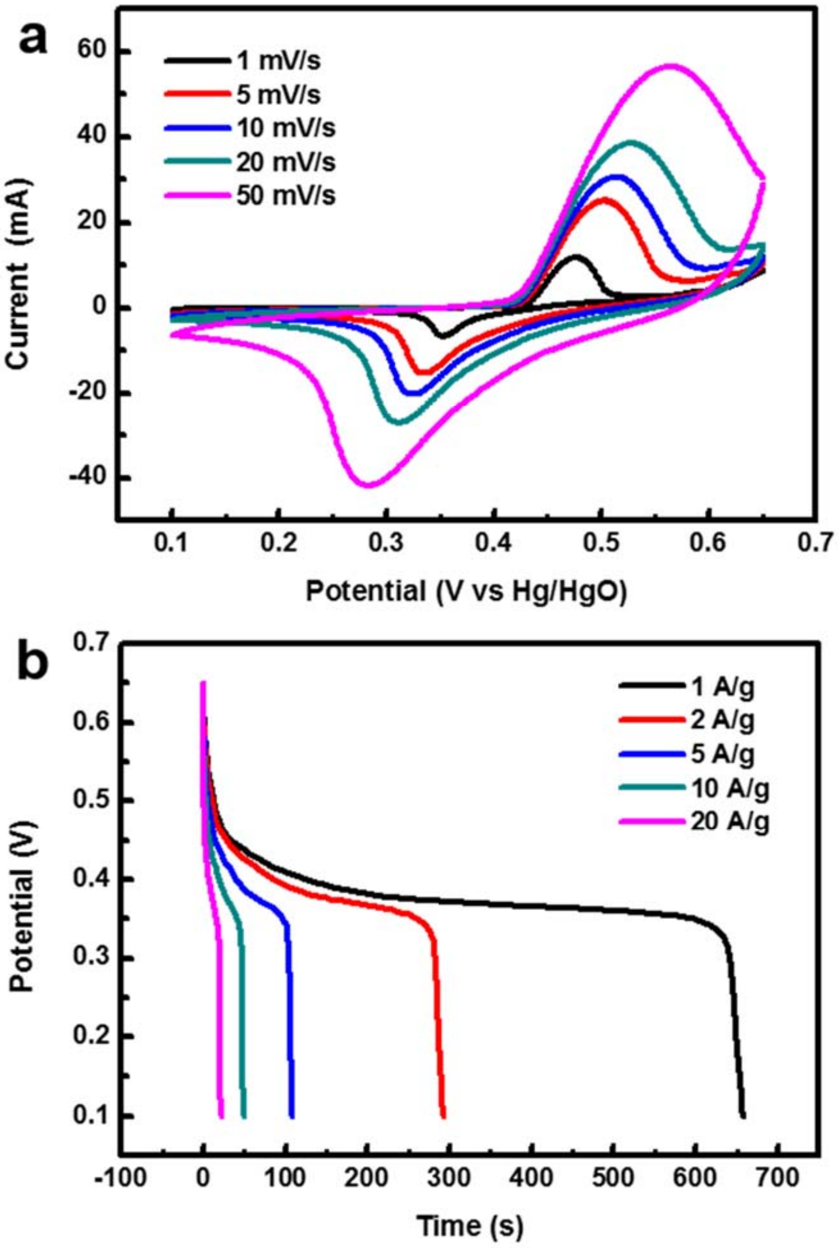

Figure S5. (a) Cyclic voltammograms of NiSCC-Ni(OH)$_2$ within the potential window from 0.1 to 0.65 V (vs Hg/HgO) at various scan rate (b) Galvanostatic discharge curves of Ni(OH)$_2$ measured from 1 A/g to 20 A/g.

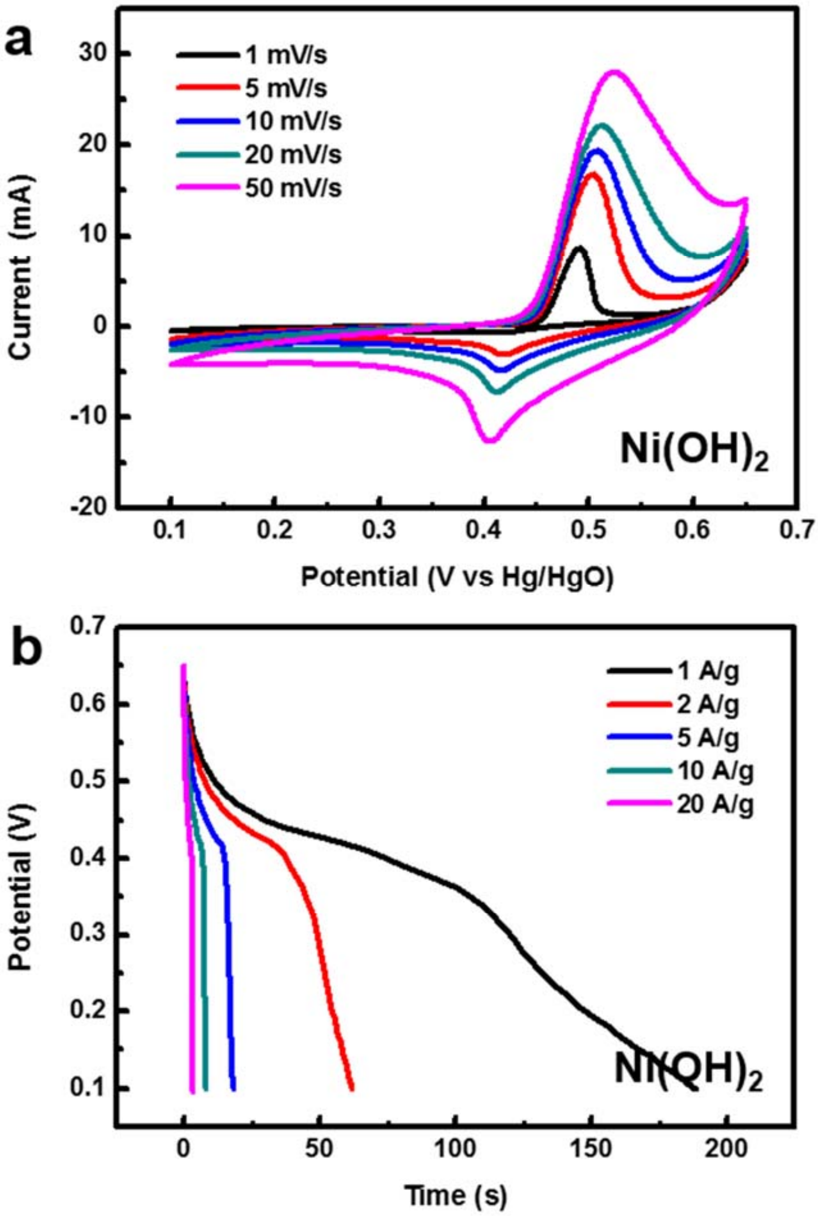

Figure S6. (a) Cyclic voltammograms of $Ni(OH)_2$ within the potential window from 0.1 to 0.65 V (vs Hg/HgO) at various scan rate (b) Galvanostatic discharge curves of $Ni(OH)_2$ measured from 1 A/g to 20 A/g.

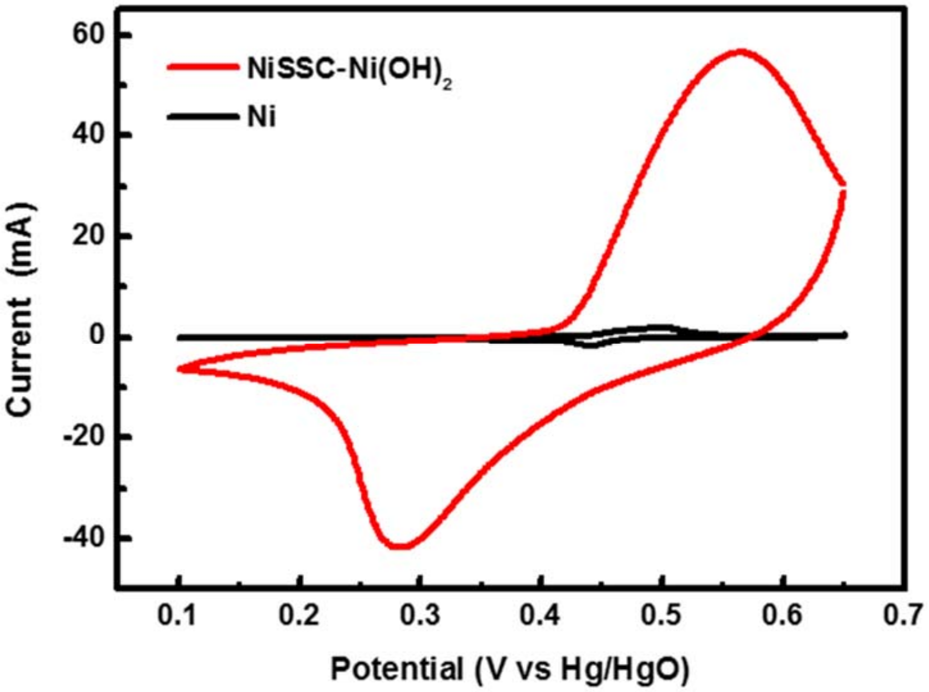

Figure S7. Cyclic voltammograms of the electrode based on Ni without active materials, $Ni(OH)_2$, and the electrode based on Ni with $Ni(OH)_2$ at 50 mV/s.

Table S1. The capacitance, kinetic property, and cycle stability of $Ni(OH)_2$ electrodes on Ni-foam in other studies

	Journal	**Active materials**	**Capacitance (F/g)**	**Kinetic Property**	**Cycle stability**
Ni-foam	Electrochimica Acta **56** (2011) 2627	$Ni(OH)_2$/NiOOH on Ni foam	1,420 F/g (2 A/g)	1,098 F/g (40 A/g)	81% (**1,000** cycle) 81%
	International Journal of hydrogen energy **36** (2011) 8674	β-$Ni(OH)_2$ nanoparticles on Ni form	1,056.1 F/g (2 mV/s)	652.8 F/g (25 mV/s)	-
	J Solid State Electrochem **13** (2009) 333	Loosed-packed $Ni(OH)_2$ nanoflake on Ni form	2,055 F/g (5 mA)	1,486 F/g (30 mA)	726.76 F/g (**1,500** cycle) 35.3%
	Chem Comm **47** (2011) 9651	β-$Ni(OH)_2$ nanowall on Ni form	2,675 F/g (5 mA/cm^2) 7.85 F/cm^2 (5 mA/cm^2)	3.41 F/cm^2 43% (30 mA)	96% (**500** cycle)
Ni-SCC	In this study	$Ni(OH)_2$ with supporting current collector	1,264 F/g (1A/g)	906 F/g (20A/g)	75% (**10,000** cycle)

Table S2. The calculated capacitance w/wo counting NiSCC as active materials

Ni-deposition time	Capacitance (F/g) ignoring NiSCC as active materials	Capacitance (F/g) including NiSCC as active materials
No deposition	363 F/g	363 F/g
1 min	870 F/g	775 F/g
1 min 30S	1,136 F/g	927 F/g
2 min	1,264 F/g	967 F/g
3 min	1,412 F/g	942 F/g

All the capacitance values were greatly improved after Ni-deposition even when we considered NiSCCs as active materials.